Crystal Structure of a Porous Zirconium Phosphate/Phosphonate Compound and Photocatalytic Hydrogen Production from Related Materials

Houston Byrd,[†,§] Abraham Clearfield,*[,‡] Damodara Poojary,[‡] Kenneth P. Reis,[†] and Mark E. Thompson*[,†]

Department of Chemistry, University of Southern California, Los Angeles, California 90089, and Department of Chemistry, Texas A&M University, College Station, Texas 77843

Received January 17, 1996. Revised Manuscript Received May 24, 1996[⊗]

The preparation, structure, and catalytic properties of porous zirconium phosphate/phosphonate compounds are discussed. The crystal structure for the $Zr_2(PO_4)(O_3PCH_2CH_2(viologen)CH_2CH_2PO_3)X_3{\cdot}3H_2O$, X = halide, is presented. The structure was determined ab initio from X-ray powder diffraction data and refined by Rietveld methods. The compound crystallizes with the symmetry of space group *P*2/*c* with $a = 13.589(2)$ Å, $b = 8.8351(9)$ Å, $c = 9.229(1)$ Å, and $\beta = 100.79°$. The structure consists of inorganic lamellae bridged by phosphono−ethyl−viologen groups. Large pores are formed in this material, which contain one halide ion and three water molecules per formula unit. The free halide ions in these materials are readily exchanged for $PtCl_4^{2-}$ ions. The Pt salt was reduced to give fine metal particles inside the porous solid. These materials produce hydrogen photochemically from water using ultraviolet light. The average rate of H_2 production is 0.15 mL/h with a lower limit quantum yield of 4% based only on the ultraviolet portion of the spectrum in the presence of a sacrificial reductant (EDTA).

Introduction

The structural control of molecular materials is an expansive area of research. To make materials with predetermined properties, molecular species need to be arranged in the bulk solid state in a manner that enhances the desired physical properties of the molecules. A wide range of techniques have been explored to prepare molecular materials with a specific alignment in the bulk.[1−5] A technique that can lead to well-ordered, thermally stable materials involves the formation of lamellar metal/organic compounds, such as transition-metal phosphonates.[6] These metal phosphonates can be prepared with a large variety of organic groups, leading to materials with a wide range of properties.[6,7]

While a wide variety of structures have been formed with molecular materials, leading to interesting electronic, optical, or magnetic properties, their use as catalysts are very limited. In the majority of these molecular materials, the solids are dense, and only the surfaces of the particles are accessible to external reagents or substrates. In contrast, inorganic frameworks can be used to construct many microporous materials,[8−12] with very open structures, which allow reagents or substrates to access the majority of the solid.

† University of Southern California.
‡ Texas A&M University.
§ Permanent address: Department of Chemistry, Montevallo University, Montevallo, AL 35115.
* To whom correspondence should be addressed.
⊗ Abstract published in *Advance ACS Abstracts,* August 1, 1996.

(1) (a) Etter, M. C. *Acc. Chem. Res.* **1990**, *23*, 120−126 and references therein. (b) Panunto, T. W.; Urbanczk-Lipkowska, Z.; Johnson, R.; Etter, M. C. *J. Am. Chem. Soc.* **1987**, *109*, 7786. (c) Etter, M. C.; Frankenbach, G. M. *Chem. Mater.* **1989**, *1*, 10. (d) Folkers, J. P.; Zerkowski, J. A.; Laibinis, C. T.; Seto, T.; Whitesides, G. M. *ACS Symp. Ser.* **1992**, *499*, 10−23 and references therein.

(2) (a) Chiang, W.; Ho, D. M.; Van Engen, D.; Thompson, M. E. *Inorg. Chem.* **1993**, *32*, 2886−2893. (b) Stults, B. R.; Marianelli, R. S.; Day, V. W. *Inorg. Chem.* **1975**, *14*, 722. (c) Cesari, M.; Neri, C.; Perotti, E.; Zazzetta, A. *J. Chem. Soc., Chem Commun.* **1970**, 276. (d) Mathew, M.; Carty, A. J.; Palenik, G. J. *J. Am. Chem. Soc.* **1970**, *92*, 3197. (e) Hanack, M.; Deger, S.; Keppler, U.; Lange, A.; Leverenz, A.; Rein, M. *Synth. Met.* **1987**, *19*, 739. (f) Pollagi, T. P.; Stoner, T. C.; Dallinger, R. F.; Gilbert, T. M.; Hopkins, M. D. *J. Am. Chem. Soc.* **1991**, *113*, 703. (g) Chisholm, M. H.; Hoffman, D. M.; Huffman, J. C. *Inorg. Chem.* **1983**, *22*, 2903.

(3) (a) Whittingham, M. S.; Jacobson, A. J. *Intercalation Chemistry*; Academic Press: New York, 1982. (b) Schollhorn, R. In *Inclusion Compounds*; Atwood, J. L., Davies, J. E. D., MacNicol, D. D., Eds.; Academic: London, 1984; Vol. 1, Chapter 7. (c) *Reactivity of Solids and Layered Compounds*; American Chemical Society Meeting, New York, April 1986; *Solid State Ionics* **1986**, *22*, 1−148.

(4) (a) *Molecular Engineering in Ultrathin Polymeric Films*; Stroeve, P., Franses, Eds.; Elsevier Applied Science: London, 1987; reprinted from *Thin Solid Films* **1987**, *152 (1, 2)*. (b) Kuhn, H. *Pure Appl. Chem.* **1981**, *53*, 2105−2122. (c) Möbius, D. *Can. J. Phys,* **1990**, *68*, 992. (d) Metzger, R. M.; Wiser, D. C.; Laidlaw, R. K.; Takassi, M. A. *Langmuir* **1990**, *6*, 350−357.

(5) (a) Ulman, A. *An Intorduction to Ultrathin Organic Films: from Langmiur-Blodgett to Self Assembly*; Academic Press: Boston, 1991. (b) Laibinis, P. E.; Whitesides, G. M.; Allara, D. L.; Tao, Y.-T.; Parikh, A. N.; Nuzzo, R. G. *J. Am. Chem. Soc.* **1991**, *113*, 7152−7167. (c) Laibinis, P. E.; Whitesides, G. M. *J. Am. Chem. Soc.* **1992**, *114*, 1990−1995. (d) Finklea, H. O.; Avery, S.; Lynch, M.; Furtsch, T. *Langmuir* **1987**, *3*, 409−413. (h) Poojary, D. M.; Zhang, B.; Clearfield, A. *Angew. Chem., Int. Ed. Engl.* **1994**, *33*, 2324. (i) Oritz-Avila, C. Y.; Bhardwaj, C.; Clearfield, A. *Inorg. Chem.* **1994**, *333*, 2499.

(6) Thompson, M. E. *Chem. Mater.* **1994**, *6*, 1168−1175.

(7) (a) Alberti, G.; Costantino, U.; Allulli, S. Tomassini, N. *J. Inorg. Nucl. Chem.* **1978**, *40*, 1113−1117. (b) Dines, M. B.; DiGiacomo, P. M. *Inorg. Chem.* **1981**, *20*, 92−97. (c) Dines, M. B.; Griffith, P. C. *Inorg. Chem.* **1983**, *22*, 567−569. (d) DiGiacomo, P. M.; Dines, M. B. *Polyhedron* **1982**, *1*, 61−68. (e) Dines, M. B.; Griffith, P. C. *Polyhedron* **1983**, *2*, 607−611. (f) Alberti, G.; Costantino, U. *Inclusion Compounds, Inorganic and Physical Aspects of Inclusion*; Atwood, J. L., Davies, J. E. D., MacNicol, D. D., Eds.; Oxford University Press: Oxford, 1991; Chapter 5. (g) Troup, J. M.; Clearfield, A. *Inorg. Chem.* **1977**, *16*, 3311−3314.

(8) Barrer, R. M. *Hydrothermal Chemistry of Zeolites*; Academic Press: New York, 1982.

(9) Suib, S. L. *Chem. Rev.* **1993**, *93*.

(10) Smith, J. V. *Chem. Rev.* **1988**, *88*, 149.

(11) Mortier, W. J.; Schoonheydt, R. A. *Prog. Solid State Chem.* **1985**, *16*, 1.

(12) Ocelli, M. L.; Robson, H. E. *A.C.S. Symp. Ser.* **1989**, *398*.

S0897-4756(96)00030-0 CCC: $12.00

These inorganic materials have many important applications, including ion exchange[13] and heterogeneous catalysis.[14,15] Metal phosphonates can also be constructed as porous compounds[16,17] and potentially used as heterogeneous catalysts. To make porous metal phosphonates, a mixture of monophosphonic (or phosphoric) acids and diphosphonic acids are used in the synthesis (eq 1). Most of the porous metal phosphonate

$$Zr^{4+} + (1 - x)H_2O_3P{-}R{-}PO_3H_2 + 2xH_2O_3P{-}R' \rightarrow Zr(O_3P{-}R')_{2x}(O_3P{-}R{-}PO_3)_{1-x} \quad (1)$$

materials use organic pillaring agents which are inert.[6] The main purpose of the pillaring agent in the materials prepared thus far is to act as structural members, holding the inorganic layers apart. However, porous metal phosphonates have recently been prepared in which the organic pillars are quite active.[6,16] Therefore, one can envision designing new solid-state materials with exciting properties by controlling the organic moieties incorporated into the pillars.

In this paper we report the preparation of new porous metal phosphonate compounds and the crystal structure of one of these materials. The structure was determined from synchrotron powder diffraction data. The refined Rietveld formula for this compound is $Zr_2(PO_4)(O_3PCH_2CH_2(viologen)CH_2CH_2PO_3)X_3{\cdot}3H_2O$, X = halide. The structure consists of metal phosphate/phosphonate lamellae, bridged by alkylviologen groups. Large pores are formed in this material, which contain one halide ion and three waters per formula unit. This free halide can readily be exchanged for $PtCl_4^{2-}$ ions, and the Pt salt reduced to give colloidal metal particles inside the porous solid. By taking advantage of the photoinduced charge-separated state observed in this porous material and related compounds, we have been able to produce hydrogen gas from an aqueous system in the presence of a sacrificial reductant (EDTA).

Experimental Section

Materials. Zirconium(IV) oxychloride octahydrate ($ZrOCl_2{\cdot}8H_2O$, Aldrich), 85% orthophosphoric acid (H_3PO_4, Fisher Scientific), 2-carboxyethylphosphonic acid (Aldrich), and 51% hydrofluoric acid (HF, Fisher Scientific) were used as purchased without further purification. Viologen bisphosphonic acid (PV) was prepared via the Michaelis−Arbuzov[18] reaction and has been reported previously.[19,20]

Instrumentation. FTIR spectra were obtained (KBr pellets) using a Nicolet 730 FTIR spectrometer. Powder X-ray diffraction measurements were obtained at ambient temperatures using a Scintag XDS 2000 automated powder diffractometer with Cu Kα radiation and a solid-state detector. The data were collected over the angular range $2° \le 2\theta \le 60°$ at a rate of 2°/min. Photolysis of materials were performed with a 200 W mercury−xenon arc lamp (Spectral Energy Corp., Westwood, NJ). Production of hydrogen gas was measured using a Hewlett-Packard 5890 Series II gas chromatograph. The amount of hydrogen was measured as a percentage of a known hydrogen standard (5% H_2, balance N_2) and then multiplied by the free volume of the irradiated cell.

Electron probe microanalysis (EPMA) was performed on a CAMECA SX-50. Conditions for collecting X-ray microanalytical data included an accelerating voltage of 15 kV, a regulated beam current of 20 nA, and a defocused electron probe 10 μm in diameter. The following reference compounds and minerals were used as calibration standards: ZrO_2 (Zr Lα), $Ca_5(PO_4)_3F$ (P Kα), Pt (Pt Mα), along with Si or $CaSiO_3$ (Si Kα) depending upon the substrate composition. Matrix corrections were performed using the $\Phi(\rho,Z)$ method.

Synthesis of Zirconium(phosphate)bisethylviologen Phosphonate {$Zr_2(PO_4)PVX_3$}. This compound has been prepared in a manner similar to that reported previously.[16] In a round-bottom flask, 1.12 mM of $ZrOCl_2$ was added to 25 mL of water followed by adding 4.72 mmol of HF (51%) solution. A solution of 0.56 mmol of *N*,*N*′-bis(2-phosphonoethyl)-4,4′-bipyridine (PV) and 1.12 mmol of 85% orthophosphoric acid (POH) dissolved in 25 mL of water was slowly added to the Zr/HF solution while stirring. The mixture was then heated under reflux conditions. After about 3 h, a white precipitate forms. Refluxing was continued for a period of 7 days. After refluxing, the solid was filtered and washed with water and then acetone before being air-dried. This material has also been prepared from a 50/50 butanol/water solvent system. Powder X-ray and IR data agree with those reported previously.[16]

Hydrothermal Synthesis of $Zr_2(PO_4)PVX_3$. In a Teflon-lined acid digestion bomb, 1.14 mmol of $ZrOCl_2{\cdot}8H_2O$, 14.8 mmol of HF, 0.55 mmol of PV, and 1.34 mmol of H_3PO_4 were added to 17 mL of H_2O. The bomb was sealed and placed in an oven and heated to 195 °C (±5 °C) for 5 days. The resulting microcrystalline powder was filtered and washed with water, ethanol, and acetone and air-dried. The powder X-ray diffraction pattern for this material is shown in Figure 1.

Platinum Exchange. Typically, 200 mg of the porous compound was placed in 20 mL of a 5×10^{-3} M solution of K_2PtCl_4 and heated at 65 °C for 18−24 h. The solution was not exposed to light to limit the degradation of the salts to metal colloids. The exchanged compounds are then filtered and rinsed with water and acetone. The Pt^{2+} ions are then reduced to Pt^0 by suspending the exchanged compound in water and bubbling H_2 gas through the solution for 2 h at 60 °C. The Pt-reduced materials are filtered and washed with water and acetone before being air-dried.

X-ray Data Collection, Structure Solution, and Refinement of $Zr(PO_4)PV$. Step-scanned X-ray powder data for the sample of $Zr_2(PO_4)PVX_3$ (side-loaded into a flat aluminum sample holder) were collected on the finely ground sample by means of a Rigaku computer-automated diffractometer. The X-ray source was a rotating anode operating at 50 kV and 180 mA with a copper target and graphite monochromatic radiation. Data were collected between 3° and 70° in 2θ with a step size of 0.02° and a count time of 25 s/step. Data were mathematically stripped of the $K\alpha_2$ contribution and peak picking was conducted by a modification of the double-derivative method.[21] The powder pattern was indexed by Ito methods[22a] on the basis of the first 20 observed lines. The best solution, which indexed all the lines yielded a monoclinic cell with systematic absences consistent with the space group *P*2/*c*. The unit-cell dimensions except the interlayer spacing (*a* axis) are similar to that found for a mixed Zr phosphate/phosphonate compound (Zr phosphate/PMIDA)[23] whose structure was determined previously from synchrotron powder

(13) (a) Breck, D. W. *Zeolite Molecular Sieves*; Kreiger: Malabar, FL, 1974. (b) Meier, W. M.; Olson, D. H. *Atlas of Zeolite Structure Types*; Butterworth: London, 1987.
(14) Imelik, B.; et. al. *Catalysis of Solids*; Elsevier: New York, 1980 and references therein.
(15) (a) Lago, R. M. U.S. Patent 4,025,572, Mobil, 1977. (b) Flanigen, E. M.; Bennett, J. W.; Grose, R. W.; Cohen, J. D.; Patton, R. L.; Krichner, R. M.; Smith, J. V. *Nature* **1978**, *271*, 512.
(16) Vermeulen, L. A.; Thompson, M. E. *Chem. Mater.* **1994**, *6*, 77−81.
(17) (a) Dines, M. B.; Cooksey, R. E.; Griffith, P. C.; Lane, R. H. *Inorg. Chem.* **1983**, *22*, 1004−1006. (c) Alberti, G.; Costantino, U.; Vivani, R.; Zappelli, P. *Mater. Res. Soc. Symp. Proc.* **1991** *233*, 95 and references therein. (d) Wang, J. D.; Clearfield, A. *Mater. Chem. Phys.* **1993**, *35*, 208−219 and references therein. (e) Yang, C. Y.; Clearfield, A. *React. Polym.* **1987**, *5*, 13−21. (f) Clearfield, A. *J. Mol. Catal.* **1984**, 251−262. (g) Clearfield, A. *Comments Inorg. Chem.* **1990**, *10*, 89−128.
(18) Bhattacharaya, A. K.; Thyagarajan, G. *Chem. Rev.* **1981**, *81*, 415−430.
(19) Vermeulen, L. A.; Snover, J. L.; Sapochak, L. S.; Thompson, M. E. *J. Am. Chem. Soc.* **1993**, *115*, 11767−11774.
(20) Snover, J. L.; Byrd, H.; Suponeva, E. P.; Vicenzi, E.; Thompson, M. E. *Chem. Mater.*, in press.
(21) Mellory, C. L.; Snyder, R. L. *Adv. X-ray Anal.* **1979**, *23*, 121.
(22) (a) Visser, J. W. J. *Appl. Crystallogr.* **1969**, *2*, 89. (b) Rudolf, P. R.; Clearfield, A. *Inorg. Chem.* **1989**, *28*, 1706.

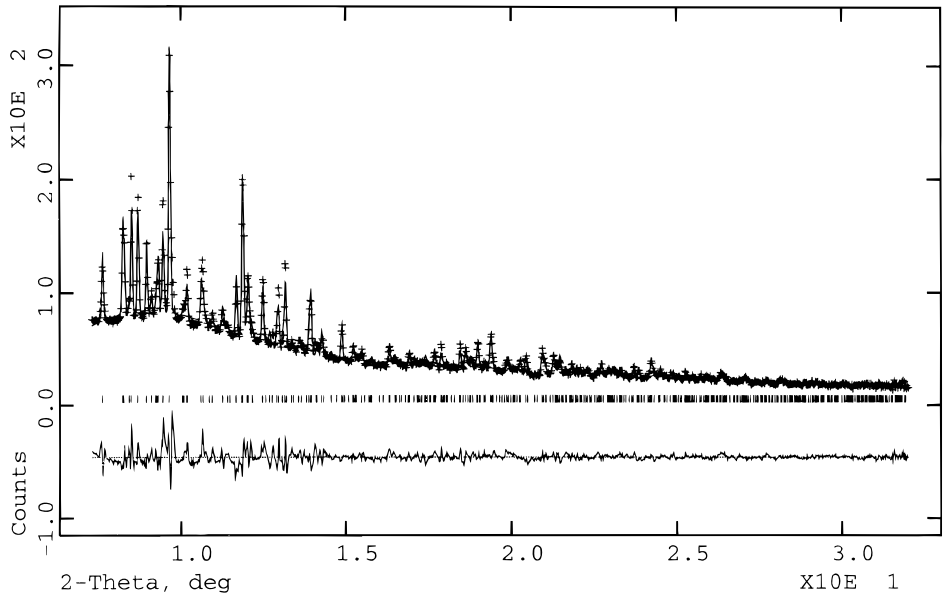

Figure 1. Observed (+) and calculated (−) profiles (X-ray intensity versus 2q) for the Rietveld refinement. The bottom curve is the difference plot on the same scale. Data were collected using the synchrotron light source (λ = 0.655 37 Å).

diffraction data. Although the phosphonate in this case contains a bulky carboxylate complex and it does not bridge the layers as in the present case, the unit cells were similar.

Synchrotron X-ray powder diffraction data were collected in capillary mode,[24] using a linear position sensitive detector[25] at the X-7A beamline at the National Synchrotron Light Source, Brookhaven National Laboratory. The wavelength (λ = 0.655 37(5) Å) was calibrated using a CeO_2 standard (a = 5.4113(1) Å). 2θ diffraction angles from 5 to 32.25 were scanned through step intervals of 0.5° on the PSD with counting times of 20 s/step. The central 3° of the PSD was binned to avoid parallax problems. The powdered sample was sealed in a 0.3 mm diameter quartz capillary. The sample capillary was rotated during data collection in order to mitigate against preferred orientation and to improve powder statistics.

Structure Solution. Interacted intensities were extracted from the profile over the range 3° < 2θ < 50° by decomposition methods as described earlier.[22b] This procedure produced 43 single indexed reflections and 15 peaks with two or three contributors. The intensities of the latter set of peaks were divided equally between the number of contributing reflections and added to the starting data set. A Patterson map was computed using this data set in the TEXSAN[26a] series of single-crystal programs. The positions of the Zr atom and that of the P atoms were derived from this Patterson map. Interestingly, these positions were similar to the Zr and P positions in the phosphonate/PMIDA compound.[23] The inorganic layer structure in the Zr phosphate/PMIDA compound was therefore used for Rietveld refinement and structure completion.

For the Rietveld refinement, the raw powder data were transferred to the GSAS[26b] program package for full-pattern refinement. After the initial refinement of scale, background, and unit-cell constants, the atomic positions were refined with soft constraints for Zr and P polyhedra. From the difference Fourier maps and model building, the positions of the carbon atoms of the viologen group were derived which were then included in the structural model. The agreement between the observed and calculated powder profiles improved significantly and a series of subsequent difference Fourier maps allowed the positioning of all the lattice water molecules and the charge-neutralizing F atom. Final refinement was carried out with soft constraints for all the atoms whose weight was reduced as the refinement progressed. These soft constraints could not be removed completely without reducing the stability of the refinement. The thermal parameters for all the atoms were refined isotropically. Neutral atomic scattering factors were used for all atoms.[26b] Corrections were made for preferred orientation effects but not for anomalous dispersion and absorption. The crystal data are given in Table 1, and the atom positions are given in Table 2. The observed (+) and calculated (−) profiles (X-ray intensity versus 2θ) for the Rietveld refinement are shown in Figure 1.

Table 1. Crystal Data for $Zr_2(PO_4)PVX_3$

space group	$P2/c$
2θ range	7.3−32°
radiation	synchrotron
wavelength	0.65537 Å
a	13.5895(22) Å
b	8.8351(9) Å
c	9.2294(10) Å
β	100.79°
expected wRp	0.022
wRp	0.08
Rp	0.062
RF	0.15

Hydrogen Production. In these experiments 25 mg of the reduced compound and 5 mL of a 0.1 M EDTA solution were placed in a 1 cm × 7 cm quartz cuvette (a stir bar is also added). The cuvette is sealed with Teflon/rubber septum and purged with N_2. The amount of time spent purging the system is important to the hydrogen production. For the best results, N_2 was bubbled through the EDTA/compound suspension for more than 45 min. Photolysis of the compound was carried out with an unfiltered 200 W Hg/Xe lamp. The lamp irradiates a 2 cm length of the cell. The lamp intensity at the sample was estimated using cutoff filters and a silicon radiometer. The intensity of the lamp below 320 nm was estimated to be 15−20 mW/cm^2, while the intensity between 320 and 800 was roughly 200 mW/cm^2. Hydrogen gas production was monitored by gas chromatography. A 0.5 mL gas sample was removed from the sealed cell and injected into the gas chromatograph. The area of the hydrogen peak is compared to a standard 5% hydrogen gas mixture (balance nitrogen).

Results and Discussion

Structure of the Porous Compounds. A layered structure is the most common motif for the tetravalent

(23) Poojary, D. M.; Zhang, B.; Clearfield, A. *Angew. Chem., Int. Ed. Engl.* **1994**, *33*, 2324−2326.

(24) Cox, D. E.; Toby, B. H.; Eddy, M. M. *Aust. J. Phys.* **1988**, *41*, 117. Cox, D. E. *Synchrotron Radiation Crystallography*; Academic Press: London, 1992.

(25) Smith, G. C. *Synch. Radiat. News* **1991**, *4*, 24.

(26) (a) TEXSAN Structure analysis package, Molecular Structure Corp., The Woodlands, TX, 1987 (revised). (b) GSAS: Generalized Structure Analysis System; Larson, A., von Dreele, R. B., Eds.; LANSCE, Los Alamos National Laboratory, copyright 1985−88 by the Regents of the University of California.

Table 2. Atom Positions for $Zr_2(PO_4)PVX_3$

atom	*X*	*Y*	*Z*
ZR1	0.1099(10)	0.2533(12)	0.0705(12)
P1	0.1294(14)	0.1174(18)	0.4295(17)
O1	0.1537(18)	0.1527(20)	0.2769(16)
O4	0.0660(15)	0.4400(15)	0.1698(25)
O5	0.0652(19)	0.3485(21)	0.1331(20)
O2	0.1517(18)	0.0517(13)	0.4789(21)
O3	0.0209(12)	0.1488(23)	0.4384(32)
C1	0.1943(24)	0.2540(24)	0.5564(27)
F1	0.2509(12)	0.3339(24)	0.0814(30)
P2	0.0000000(0)	0.5423(22)	0.2500000(0)
C2	0.2238(14)	0.211(4)	0.7170(24)
N1	0.3347(13)	0.1658(30)	0.7232(22)
C3	0.3491(11)	0.0064(29)	0.7177(20)
C4	0.4003(8)	−0.0519(22)	0.6169(13)
C5	0.4552(10)	0.0271(17)	0.5340(17)
C6	0.4266(22)	0.1830(19)	0.5291(23)
C7	0.3966(19)	0.2463(25)	0.6549(26)
O(W1)	0.4101(19)	0.3478(24)	0.9527(32)
O(W2)	0.300(4)	0.5088(32)	0.789(4)
F2	0.5000000(0)	0.303(4)	0.2500000(0)

bond	bond distance
Zr1−O1	2.085(13)
Zr1−O4	2.030(12)
Zr1−O5	2.044(13)
Zr1−O2	2.095(13)
Zr1−O3	1.992(14)
Zr1−F1	2.029(14)
P1−O1	1.53815)
P1−O2	1.574(15)
P1−O3	1.517(16)
P1−C1	1.795(16)
P2−O5	1.588(13)
P2−O4	1.555(12)

bond	angle
O1−Zr1−O4	89.5(7)
O1−Zr1−O5	178.9(9)
O1−Zr1−O2	87.3(7)
O1−Zr1−O3	86.6(7)
O1−Zr1−F1	90.0(8)
O4−Zr1−O5	91.1(7)
O4−Zr1−O2	176.1(9)
O4−Zr1−O3	93.4(8)
O4−Zr1−F1	92.7(8)
O5−Zr1−O2	92.0(7)
O5−Zr1−O3	92.5(8)
O5−Zr1−F1	91.0(8)
O2−Zr1−O3	84.0(9)
O2−Zr1−F1	89.6(8)
O3−Zr1−F1	172.9(10)
O1−P1−O2	113.2(13)
O1−P1−O3	113.0(13)
O1−P1−C1	107.3(12)
O2−P1−O3	107.1(12)
O2−P1−C1	113.9(11)
O3−P1−C1	101.9(13)
O4−P2−O4	108.9(15)
O4−P2−O5	109.1(6)
O4−P2−O5	112.3(10)
O4−P2−O5	112.3(10)
O4−P2−O5	109.1(6)
O5−P2−O5	105.2(22)

metal phosphonates.[6] In these types of solids, inorganic layers are formed in which metal ions are strongly bound to the phosphonate oxygens. These inorganic layers have phosphonate groups above and below the inorganic plane. The result is inorganic lamellae, which are separated by organic phosphonate groups. The bonding within the inorganic portion of these materials is very similar to that observed in α-$Zr(O_3POH)\cdot H_2O$.[7] The bonding between adjacent layers is strongly dependent on the phosphonate molecules and can range from weak van der Waals interactions to strong covalent

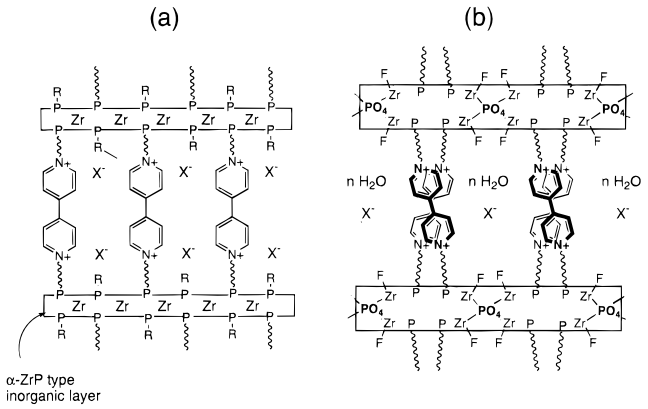

Figure 2. Schematic representation of (a) $Zr(O_3PR)PV$ and (b) $Zr_2(PO_4)PVX_3$. R = alkyl and OH. Lone "P" atoms in (b) represent $-PO_3$ groups, which are bound to three different Zr atoms.

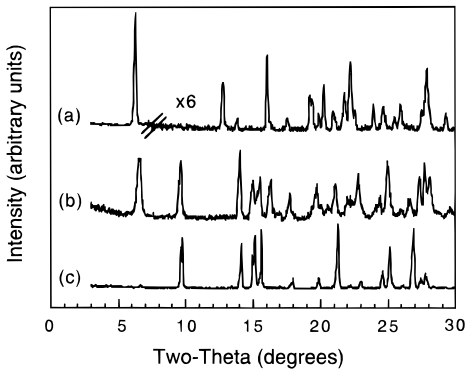

Figure 3. XRD patterns of the zirconium viologen compounds: (a) pure $Zr(PO_4)PV$; (b) mixed $Zr(PO_4)PV$/Zr*PV*(X); (c) pure Zr*PV*(X).

bonds. The strongest bonding and thus most stable structures are formed when a bisphosphonic acid is used, such that the inorganic lamellae are held together by covalent bonds.[7,17,27]

Recently, we have reported the preparation and photophysical properties of crystalline layered zirconium viologen phosphonate (Zr*PV*(X)) compounds.[19,28] The formula for this material is $(ZrF_3)_2(O_3PCH_2CH_2$-(viologen)$CH_2CH_2PO_3)\cdot H_2O$.[29] This viologen−bisphosphonic acid will be abbreviated *PV* throughout the paper. These compounds show efficient photoinduced charge separation, that is stable in air.[19,28] Zr*PV*(X) is layered but does not possess the same structural motif observed in most of the tetravalent metal phosphonate solids.[29] In Zr*PV*(X), the individual lamellae consist of both organic and inorganic components and are held together by van der Waals, electrostatic, and hydrogen bonding forces. Zr*PV*(X) layers are built from double chains of ZrF_3O_3 octahedra, which are bridged by the viologen phosphonate groups. Adjacent layers are packed with the anionic ZrF_3O_3 octahedra above and below the cationic viologen groups. This unusual structure is believed to be formed to minimize electrostatic repulsions between the viologen groups. The longevity of the charge-separated state is thought to arise from

(27) Poojary, D. M.; Hu, H. L.; Campbell, F. L.; Clearfield, A. *Acta Crystallogr.* **1993**, *B49*, 996.
(28) Vermeulen, L. A.; Thompson, M. E. *Nature* **1992**, *358*, 656−658.
(29) Poojary, D. M.; Vermeulen, L. A.; Vicenzi, E.; Clearfield, A.; Thompson, M. E. *Chem. Mater.* **1994**, *6*, 1845−1849.

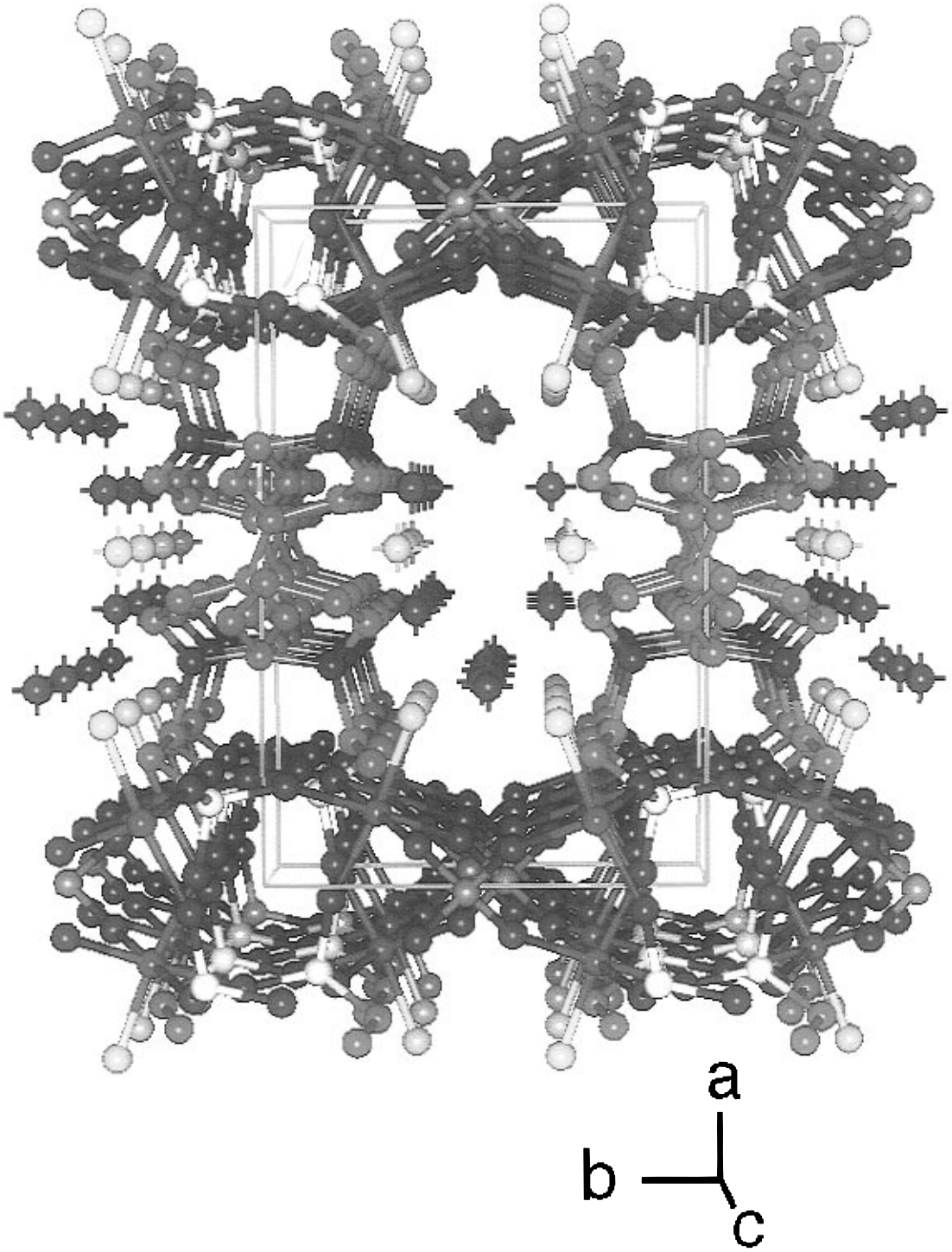

Figure 4. Structure of $Zr_2(PO_4)PVF_3$ viewed along the *c* axis (shown in perspective). Phosphate phosphorous atoms are shown in orange and *PV* phosphorous atoms are shown in gray.

the ability of the lattice to prevent diffusion of oxygen into the structure.

A family of mixed metal phosphate/viologen−phosphonate and metal phosphonate/viologen−phosphonate materials have been prepared.[16,30] A wide range of different materials of the general formula $Zr(O_3P-R'-)_{2x}(O_3P-R-PO_3)_{1-x}$ were prepared, in which the −R′ group was −OH, $-CH_2CH_2X$, X = −Br, −COOH, $-CH_3$, $-NH_2$, and the −R− group was $-(CH_2)_n-$viologen$-(CH_2)_n-$, where $n = 2, 4$ (eq 1). Most of these materials give simple powder X-ray diffraction patterns, consisting only of a series of 00*l* lines, which suggests a structure similar to that shown in Figure 2a.

In the synthesis of the mixed zirconium phosphate/phosphonate compounds involving *PV* and phosphoric acid, two different phases were observed. One of these phases showed only 00*l* reflections in the powder X-ray diffraction patterns ($d = 18$ Å), indicative of a layered structure.[16] Electron probe microanalytical (EPMA) data for this compound were consistent with the composition: $Zr(O_3POH)(O_3P-CH_2CH_2-$viologen$-CH_2-CH_2-PO_3)_{0.5}Cl$, abbreviated $Zr(O_3POH)PV$.[29] The other phase was significantly more crystalline, with a interlayer spacing of 13.5 Å. The X-ray diffraction pattern for the 13.5 Å phase is shown in Figure 1.

(30) Reis, K. P.; Runyan, C.; Thompson, M. E., unpublished results.

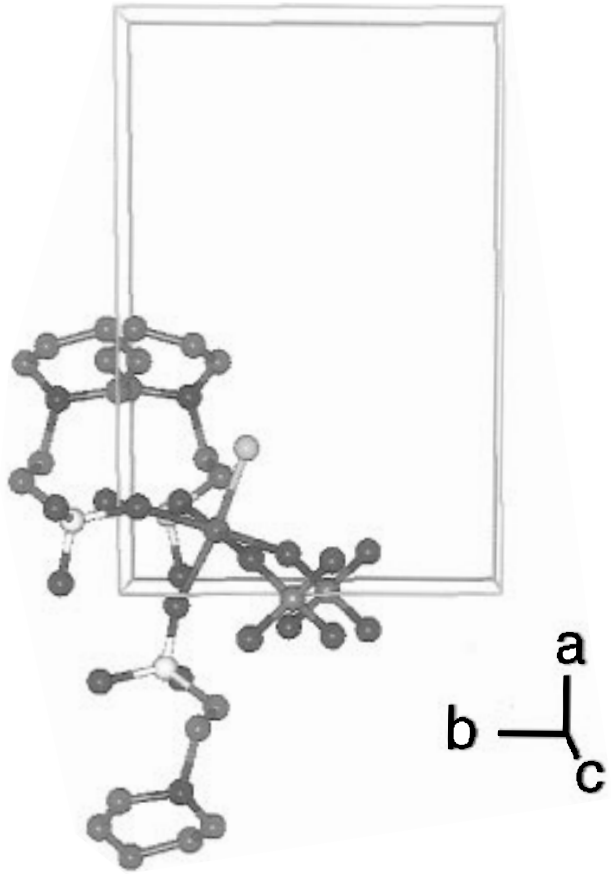

Figure 5. Portion of the $Zr_2(PO_4)PVF_3$ lattice showing the coordination geometry around Zr. Only half of each viologen group is shown for clarity. Phosphate phosphorous atoms are shown in orange and *PV* phosphorous atoms are shown in gray.

The standard synthetic procedure to obtain the compounds discussed above involves refluxing a mixture of the two acids and Zr in the presence of HF for several days, and often leads to materials which are a mixture of Zr*PV*(X) and the 13.5 Å phase (Figure 3b). Hydrothermal synthesis of the same compounds in a Teflon-lined acid digestion bomb leads to a sample that is significantly more crystalline and pure phased. We were unable to get crystals large enough for single-crystal X-ray diffraction studies, but were successful in solving the structure by ab initio methods with Rietveld analysis and refinement of powder X-ray and synchrotron diffraction data. The structure is shown schematically in Figure 2b. The stoichiometry of this crystalline phase is $Zr_2(PO_4)PVX_3{\cdot}3H_2O$, X = halide.

The structure of $Zr_2(PO_4)PVF_3{\cdot}3H_2O$ is closely related to a zirconium phosphate/phosphonate determined by Poojary et. al.[23] Atom positions as well as the bond lengths and angles for the inorganic portion of the structure are listed in Table 2. The bond lengths and angles for the ethylviologen group are within the expected range, and are given in the supporting information. The structure is shown in Figure 4, viewed down the *c* axis. The Zr atoms are octahedrally coordinated by two oxygen atoms from the phosphate groups, three oxygen atoms from the viologen phosphonate groups (in a facial geometry), and an F atom pointing into the organic layer, as shown in Figure 5. One way to picture this solid is as sheets of $(ZrF)_2PV$ lying parallel to the *ac* plane, which are bridged by rows of phosphate groups running parallel to the *c* axis. This bridging gives rise to roughly rectangular channels, running parallel to the *c* axis, seen in Figure 4. The bonding of the phosphonate groups to the Zr atoms is difficult to see in Figures 4 or 5. A view of the structure down the *a* axis (Figure 6) shows that each phosphonate group is bound to three different Zr atoms. In this view, the phosphonates are shown with only a two-carbon chain for clarity. The Zr−F bonds are labeled as to whether they are oriented out of the plane of the page (labeled u, up in Figure 6) or into the plane of the page (labeled d, down in Figure 6). The phosphonate groups form strong bonds to both sides of the inorganic lamellae. This phosphonate bonding forces the P−C bond to lie nearly parallel to the inorganic layers.

Another way to describe the structure is as inorganic lamellae, parallel to the bc plane, which are bridged by diethylviologen groups. The viologen groups in the interlamellar region form a criss-cross stack, so that electrostatic repulsions are minimized. The closest face-to-face contact between viologen groups (along *c*) is 4.6 Å. This distance is longer than the related distance in Zr*PV*(X), which is 3.5 Å.[29] The closest viologen−viologen contact across the pore (along *b*) is approximately 8 Å with a layer-to-layer distance of 13.5 Å giving rise to fairly large pores. Three water molecules and one halide ion per formula unit are found within this cavity. An alternate way of listing the compound, which emphasizes the difference between the different types of halide in the structure is $(ZrF)_2(PO_4)PVF{\cdot}3H_2O$.

The stoichiometry of this crystalline phase is $Zr_2(PO_4)PVX_3{\cdot}3H_2O$, X = halide, with fluoride being the dominant halide in the sample studied by powder X-ray diffraction. Electron probe microanalysis (EPMA) data confirmed the Zr/P ratio of 2:3. The Zr/F ratio was found to be approximately 1:1 instead of the expected 2:3. However, the discrepancy may be due to substitution of chloride for fluoride in the compound; however, this should not be significant for materials prepared by hydrothermal methods. Under refluxing conditions, the fluoride concentration gradually decreases due to evaporation of HF, leading to incorporation of reasonable amounts of chloride into the solids. The halide for the materials prepared hydrothermally is almost exclusively fluoride, since the levels of fluoride in the sealed bomb remain high throughout crystal growth. Alternatively, the low halide level could be due to inaccuracies in quantifying halides in these materials by EPMA. In analyzing Zr*PV*(X) by EPMA we found that chloride loss during microanalysis prevented us from being able to measure levels of chloride ion in the materials.[29] If the levels of Zr, P, Cl, and F are measured for the same portion of a sample of $Zr_2(PO_4)PVX_3{\cdot}3H_2O$ over time, the levels of Zr and P remain constant, while the Cl and F steadily decrease. EPMA analysis of $Zr_2(PO_4)PVX_3{\cdot}3H_2O$ was able to determine the presence of chlorine in the sample; however, precise determination of the amount of chloride or fluoride was not possible due to the loss of halide.

Solid-state ^{31}P NMR spectra of this compound showed the presence of two types of phosphate as well as the phosphonate. A very similar spectrum was reported previously and assigned to PO_4^{3-} and HPO_4^{2-}.[19] There are several ways to rationalize the presence of HPO_4^{2-} in these solids. There could be a small amount of α-$Zr(O_3POH)_2$ mixed with the porous compound, which does not show up clearly in the powder X-ray diffraction patterns. Another possibility is that some of the PO_4^{3-}

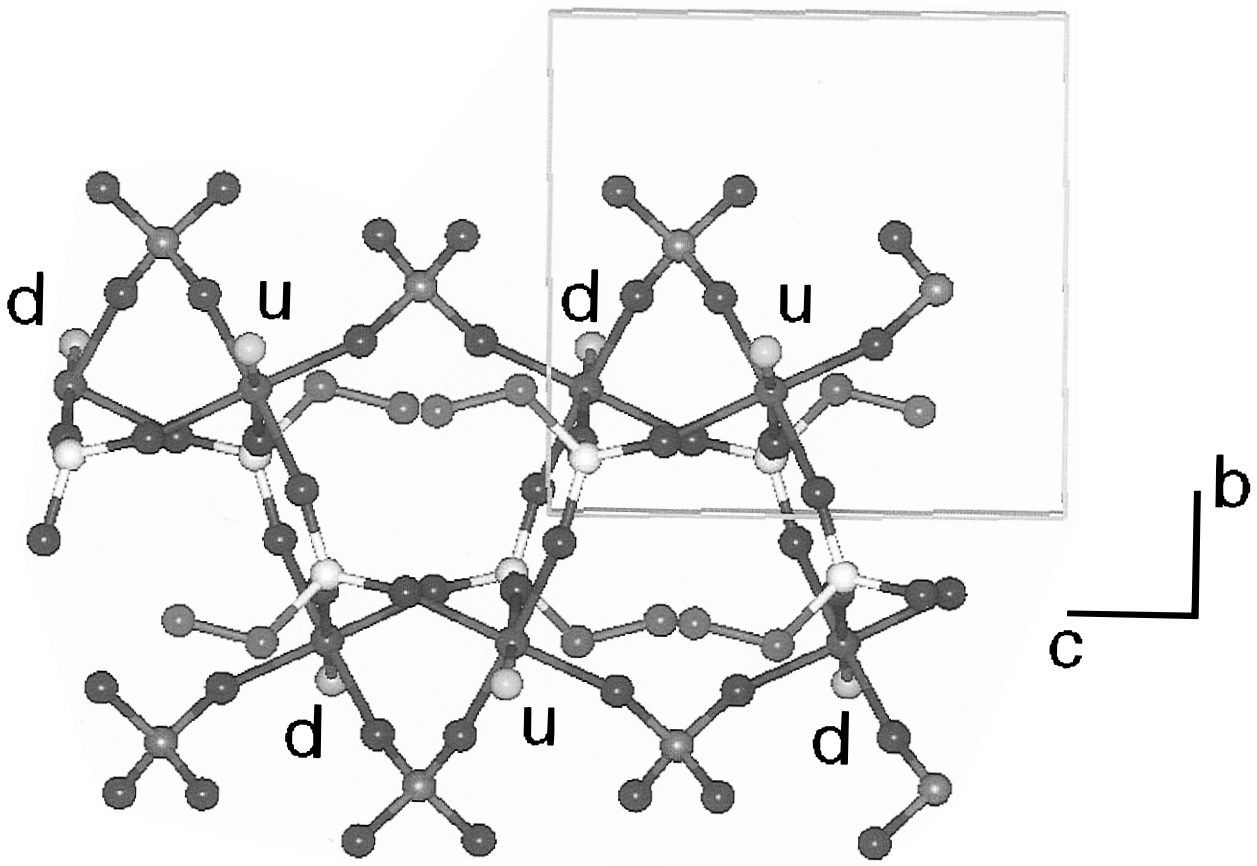

Figure 6. Portion of the $Zr_2(PO_4)PVF_3$ lattice viewed down the *b* axis. Phosphonate groups are shown in gray with only two carbons. Phosphate phosphorous atoms are shown in orange.

groups of the $Zr_2(PO_4)PVF_3$ lattice are protonated. If the level of protonation is low and the protons are distributed randomly in the lattice, their presence, or rather the structural distortion protonation would cause, would not be detected by X-ray diffraction. The protons must have associated halide ions for charge neutrality, which would presumably be in the pores.

Platinum Incorporation. Colloidal Pt particles are conveniently prepared by hydrogen reduction of $PtCl_4^{2-}$ and are known to be excellent catalysts for the reduction of water to H_2 gas.[31,32] $PtCl_4^{2-}$ can be readily incorporated into the porous materials described above by simple ion exchange for the intrapore halide ions. The initially white compounds are orange after the exchange procedure. The platinate ions are then reduced to Pt^0 by suspending the exchanged compound in water and bubbling H_2 gas through the suspension. During this process, the suspension turns a deep blue, which is an indication of the formation of reduced viologen. The extent of platinum incorporation has been monitored by ICP analysis of the dissolved solids. A Zr:Pt ratio of 4:1 is expected for complete exchange of $PtCl_4^{2-}$ into $Zr_2(PO_4)PVX_3$. Ion exchange leads to higher levels of Pt incorporation than expected, i.e., final Zr:Pt ratio of 3:1. Treatment of Zr*PV*(X) with a solution of $PtCl_4^{2-}$ gives very low levels of Pt incorporation (Zr:Pt $\approx$ 35:1) as expected for this dense solid. Ion exchange was also examined with a material which consisted of a mixture of dense and porous materials, i.e., $Zr_2(PO_4)PVX_3$/Zr*PV*(X); see Figure 3b. This material gives significantly lower levels of Pt incorporation than observed for either $Zr_2(PO_4)PVX_3$ or Zr*PV*(X); Zr:Pt levels for ion-exchanged mixed materials range from 50:1 to 100:1. Bragg reflections from Pt are not observed by powder X-ray diffraction of any of these reduced compounds.

Hydrogen Production. The photochemical splitting of water to give H_2 and O_2 is a common goal for compounds which exhibit a photoinduced charge separation.[33,34] Unfortunately, the reduction and oxidation of water are often kinetically hindered and require a catalyst to overcome these barriers. Colloidal platinum has been found to be an ideal catalyst for the reduction of water to hydrogen gas.[31,32] A sacrificial reductant (EDTA, L-cysteine, triethanolamine, etc.) can be added to an aqueous system in order to study catalytic hydrogen production independent of oxidation. A typical system for the photoreduction of water consists of a dialkylviologen, a sacrificial reductant, colloidal noble-metal particles, and a sensitizer. We have recently demonstrated such as system using a zirconium viologen bisphosphonate thin film.[35] A lower limit quantum yield of 0.8% was obtained for the photolysis of the production of hydrogen by this material.

In our photochemical studies 20−25 mg of the catalyst and 5 mL of 0.1 M EDTA solution were placed in a quartz cuvette. The cuvette was then placed in a temperature controlled (25 °C) water bath with a quartz window. Photolysis of the compound was carried out

(31) Harriman, A., West, M. A., Eds. *Photogeneration of Hydrogen*; Academic Press: London, 1982.
(32) Grätzel, M., Ed. *Energy Resources through Photochemistry and Catalysis*; Academic Press: New York, 1983.
(33) Fox, M. A.; Chanon, M., Eds. *Photoinducted Charge Transfer*; Elsevier: Amsterdam, 1988.
(34) Connolly, J. S., Ed. *Photochemical Conversion and Storage of Solar Energy*; Academic Press: New York, 1981.
(35) Snover, J. L.; Thompson, M. E. *J. Am. Chem. Soc.* **1994**, *116*, 765−766.

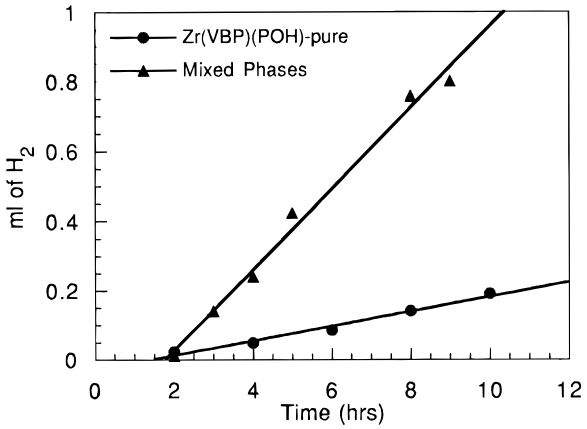

Figure 7. Hydrogen production from photolysis of compounds: (a) $Zr(PO_4)PVX_3$·Pt; (b) $[Zr(PO_4)PVX_3/ZrPV(X)]$·Pt. The rate of production ((a) 0.02 mL/ h; (b) 0.12 mL/h) is obtained from the linear regression (solid line) of the data.

with an unfiltered 200 W Hg/Xe lamp. A typical plot of the hydrogen produced versus time for the pure phased $Zr_2(PO_4)PVX_3$·Pt compound is shown in Figure 7. There is approximately a 1−2 h induction period before H_2 is observed by the GC. We speculate this period is due to residual O_2 in the cell which acts to quench the excited viologen prior to electron transfer.[36] $Zr_2(PO_4)PVX_3$·Pt gives a low rate of hydrogen production, ca. 0.02 mL/h, for several different samples. The rate of H_2 production for a mixed porous and dense phase material $[Zr_2(PO_4)$-$PVX_3/ZrPV(X)]$·Pt is significantly larger and is also shown in Figure 7, for comparison. The increase in hydrogen production is roughly a factor of 6 (0.12 mL/ h) for the material used in Figure 7. A microcrystalline sample of the dense phase material ($ZrPV(X)$) was also exchanged with Pt^{2+} ions and reduced as discussed previously. $ZrPV(X)$ is not a porous material,[29] so the exchange here must be at the surfaces of the microcrystalline particles and reduction leads to fine metal particles on the exterior of the $ZrPV(X)$ particles. The $ZrPV(X)$·Pt compound produces less than 0.005 mL/h. The reason that the mixed phase sample works better than either pure phase is not clearly understood at this time. When the pure porous materials ($Zr_2(PO_4)PVX_3$) or the pure dense material ($ZrPV(X)$) are exchanged with $PtCl_4^{2-}$ ions and reduced, the resulting compounds are very dark. The mixed-phase materials tend to be a light gray. One possible explanation is that the light does not reach the viologen moieties as efficiently for the pure (very dark) phases as it does for the mixed (gray) phases, because of light absorption by the platinum particles. Another possible explanation is that for $Zr_2(PO_4)PVX_3$·Pt and $ZrPV(X)$·Pt the platinum particles are bound to the surfaces of the particles only, so that there is very poor contact between the bulk of the viologen and the platinum particles. We are currently trying to get microanalysis at high enough resolution to determine if the platinum is uniformly distributed or concentrated at the surfaces of these microcrystalline materials.

A lower limit quantum yield for the production of hydrogen has been calculated. For this calculation, the flux of the 200 W lamp was determined for the active wavelengths of the viologen moieties (<320 nm) to be 15−20 mW/cm^2. We assume that all of the photons emitted from the lamp are absorbed by the compound. A quantum yield ($2 \times$ mol H_2/mol photons incident with $\lambda < 320$ nm) of 4% has been determined for the mixed-phase compounds using the average rate (0.15 mL/h) of hydrogen production for several samples. The rate of hydrogen production usually becomes constant after about 10 h of exposure to the light. The strong UV light eventually destroys the system after 18 h of exposure. The usefulness of these materials is limited to UV light. We are continuing to optimize the system and are trying to design materials which absorb in the middle of the visible spectrum.

Acknowledgment. The authors would like to thank The American Biomimetics Corporation and the National Science Foundation (Grant CHE-9312856) for their financial support of this work. D.M.P. and A.C. thank the National Science Foundation (Grant DMR-91107715) for financial support. Electron probe microanalysis (EPMA) was performed on a CAMECA SX-50 by Dr. Edward Vicenzi at the Princeton Materials Institute's Electron Microbeam Facility. The authors would also like to thank Professor John Parise for collecting the powder synchrotron data used to solve the structure of $Zr_2(PO_4)PVF_3$·H_2O. Professor Parise's support was provided by the National Science Foundation (DMR 94-13003). Research was carried out in part at beamline X7A, the National Synchrotron Light Source at Brookhaven National Laboratory; supported by the U.S., Department of Energy, Division of Materials Science and Division of Chemical Science.

Supporting Information Available: A complete listing of bond lengths and angles for $Zr_2(PO_4)PVF_3$·$3H_2O$ (4 pages). Ordering information is given on any current masthead page.

CM960030U

(36) An alternate explanation is that the induction period is due to slow saturation of the aqueous solution by hydrogen gas. The saturation level for H_2 for 5 mL of aqueous solution (30 °C) is 0.044 mL. For the poorer catalysts this amount of hydrogen would account for a 2 h induction period, as observed. For the better catalysts, however, the rate of hydrogen production would saturate the solution in less than 20 min, not 2 h.